Gamma Radiations of Na^{23} and Ne^{20}*

T. H. KRUSE, R. D. BENT,† AND L. J. LIDOFSKY
Columbia University, New York, New York

(Received January 18, 1960)

Na^{23} and Ne^{20} gamma rays were observed from the proton bombardment at various energies of thin evaporated Na and NaI targets and of a natural Ne gas target. Gamma rays involving Na^{23} states up to 4 Mev and Ne^{20} states up to 5 Mev were observed and decay schemes and branching ratios obtained. The 2.08- and 2.70-Mev states of Na^{23} are probably $7/2^+$ and $9/2^+$, respectively. Limitations on spin and parity values are given for other states. The results obtained for Na^{23} are consistent with the results of a strong-coupling collective calculation. The 4.97-Mev state of Ne^{20} has an upper limit for the ground-state branch of 4%. An upper limit of 9% is placed on the ground-state branch of the 4.2-Mev state of Ne^{20}. Gamma rays from the $F^{19}(d,n\gamma)Ne^{20}$ reaction were observed with energies of 11.4, 10.67, 10.16, 9.37, 8.37, and 7.36 Mev.

I. INTRODUCTION

RECENT theoretical[1] and experimental studies[2] have suggested the systematic occurrence of large nuclear equilibrium deformations in the region of mass number between O^{16} and Si^{28}. Nuclei having such deformations are expected to exhibit a low-energy collective spectrum of rotational type.[3]

The odd-even nucleus Na^{23} was excited by proton bombardment of Na, using the Columbia Van de Graaff generator. The even-even nucleus Ne^{20} was excited by the exoergic (p,α) reaction from proton bombardment of Na ($Q=+2.38$ Mev), and by proton bombardment of a natural Ne target. The de-excitation gamma rays from these reactions have been studied, using scintillation spectrometry, to provide further information on the applicability of the collective model to light nuclei. In addition, the properties of low-lying Ne^{20} states are of interest to the theories of stellar energy production and element formation.[4,5]

Gamma rays from the reaction $F^{19}+d$ were also observed. However, only those of high energy could be assigned unambiguously to Ne^{20} transitions.

II. EXPERIMENTAL APPARATUS AND PROCEDURES

1. Three-Crystal Pair Spectrometer

Concurrent detection of high-energy gamma rays was performed with a three-crystal pair spectrometer, which has been described previously.[6] Na or NaI targets were evaporated in vacuum on a backing disk of 0.005- or 0.010-inch Ta. This target was placed at the end of a thin wall Al cap, which slipped over the end of a tube at the end of the beam pipe using an "*O*" ring vacuum seal in the wall of the cap [Fig. 1(a)]. The stainless steel tube was insulated from the beam pipe with Lucite, permitting integration of the beam current. Beams of a few tenths of a microampere or less were generally employed. Gamma spectra were analyzed by a 100- or 256-channel analyzer.

2. Gamma-Gamma Coincidence Measurements

Information concerning gamma-ray cascade sequences and angular correlations was obtained by detection of the gamma-ray spectrum in coincidence with a gamma ray of a specific energy. The detectors were NaI(Tl) crystals, 3-in. diameter and 2-in. thick mounted on 5-in. Dumont 6364 photomultipliers and a 3 in.×3 in. NaI(Tl) crystal mounted on a 3-in. Dumont 6363 photomultiplier. For cascade determinations, the aluminum end cap and the tantalum target backing used

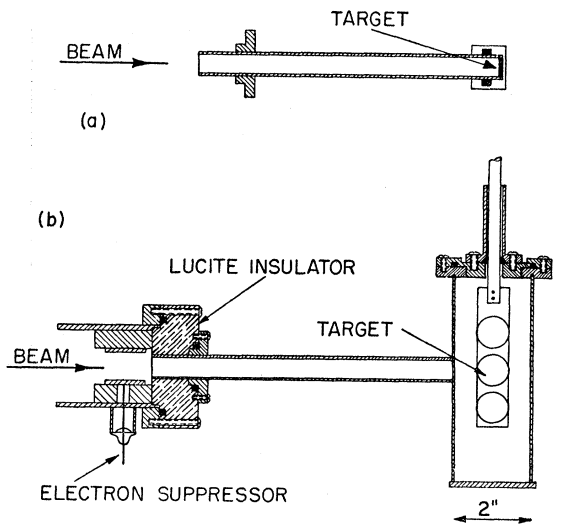

FIG. 1. (a) Target chamber used for three-crystal pair spectrometer and for gamma-gamma coincidence measurements. (b) Target chamber used for gamma-gamma angular correlation measurements.

* This work partially supported by the U. S. Atomic Energy Commission.

† Present address: Department of Physics, Indiana University, Bloomington, Indiana.

[1] G. Rakavy, Nuclear Phys. 4, 375 (1957).

[2] R. K. Sheline, Nuclear Phys. 2, 382 (1956); A. E. Litherland, H. McManus, E. B. Paul, D. A. Bromley, and H. E. Gove, Can. J. Phys. 36, 378 (1958).

[3] A. Bohr and B. R. Mottelson, Kgl. Danske Videnskab. Selskab, Mat.-fys. Medd. 27, No. 16 (1953).

[4] A. G. W. Cameron, Atomic Energy of Canada, Limited Report AECL-454, 1957 (unpublished).

[5] E. M. Burbidge, G. R. Burbidge, W. A. Fowler, and F. Hoyle, Revs. Modern Phys. 29, 547 (1957).

[6] R. D. Bent and T. H. Kruse, Phys. Rev. 108, 802 (1957).

with the three-crystal pair spectrometer were employed, with the two detectors at 90° to the beam and 180° to each other. For correlation measurements, the targets could be rotated inside a cylinder to equalize the amount of absorbing material for the two detectors. A diagram of this chamber is shown in Fig. 1(b).

A fast-slow coincidence selection scheme was used, similar to that described previously in connection with the three-crystal pair spectrometer.[6] Amplified pulses from the detectors were fed into a fast coincidence circuit. The amplified pulses from one detector were also fed into a single-channel pulse-height analyzer set to pass pulse amplitudes corresponding to the photopeak of the gamma ray of interest. The output of the single-channel analyzer was required to be in slow coincidence (2μsec) with the fast coincidence output. The slow coincidence output gated a multichannel analyzer which stored coincident pulses from the other detector.

Two fast coincidence circuits were employed on different occasions. One was that used with the three-crystal pair spectrometer, having a resolution of $2\tau=0.2$ μsec. This was used for the cascade determinations. The other, which was used for the correlation measurements, was of the Garwin type[7] with a resolution of $2\tau=30$ mμsec. When the Garwin circuit was used, pulses for analysis were taken from one of the phototube dynodes, as described below.

3. Particle-Gamma Coincidence Measurements

Heavy charged particles emitted were detected by a thin (approximately 0.015 in.) CsI(Tl) crystal mounted on a 2-in. RCA 6342 photomultiplier. Gamma rays were detected by a NaI(Tl) crystal 3 in. thick and 3 in. in diameter, mounted on a 3-in. Dumont 6363 photomultiplier. Coincidences between gamma rays and a selected group of particles produced a gating signal for the multichannel analyzer, using a fast-slow coincidence arrangement and a single-channel pulse-height analyzer as for gamma-gamma coincidences.

The particle detector was prepared by permanently mounting a CsI(Tl) disk 1/8 in. thick and 7/8-in. diameter on a thin (5/16-in.) disk of clear Lucite, using a transparent commercial bonding agent.[8] The CsI was then reduced to the required thickness by rubbing on a piece of wet silk. Na targets for use with the particle detector were prepared by evaporation of NaI onto a thin Formvar film backed by a previous evaporation of gold.

A resolution of 3 to 4% for 5-Mev protons was obtained with this detector. Magnetic shielding of the phototube was not employed. Examples of the charged particle spectra obtained from bombardment of NaI and natural Ne targets are shown in Figs. 2 and 3. Particle groups of different type (e.g., protons and alphas) were distinguished by their different pulse-height variation with bombarding energy. Charged particle groups from the various reactions were identified with energy levels of the final nuclei by their pulse heights relative to each other and to the strong elastic group and by the coincident gamma spectrum. Alpha particles were found to produce a pulse height of about 0.45 that produced by a proton having the same energy.

The target chamber employed was designed for efficient collection of data by allowing large detector solid angles. The chamber geometry is shown in Fig. 4.

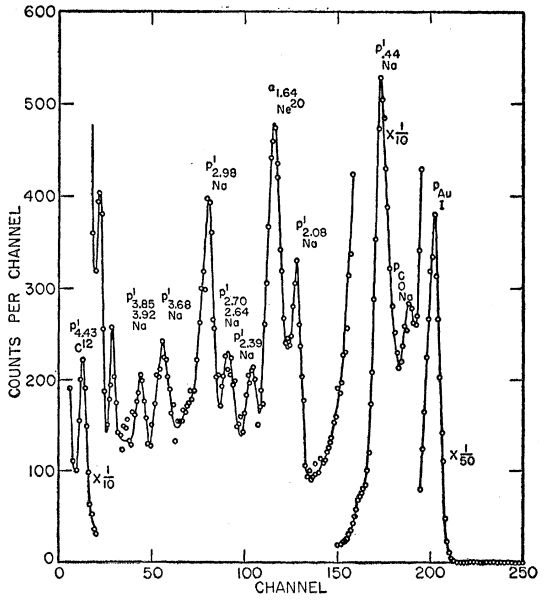

FIG. 2. Charged particle spectrum obtained with CsI(Tl) crystal from the proton bombardment of NaI at 5.54 Mev.

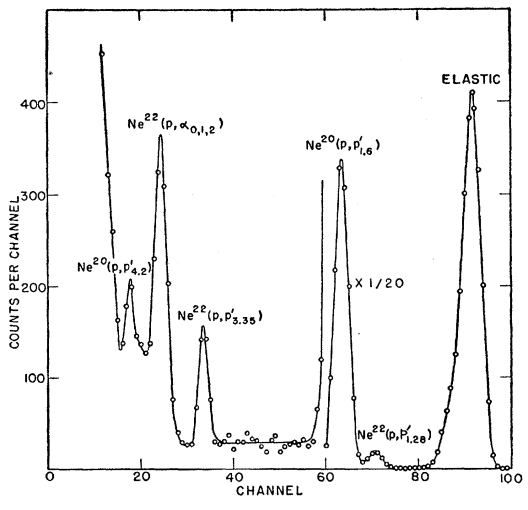

FIG. 3. Charged particle spectrum obtained with CsI(Tl) crystal from bombardment of natural Ne with 5.90-Mev protons.

[7] R. L. Garwin, Rev. Sci. Instr. **21**, 569 (1950).

[8] Helix Bonding Agent R-313, Carl H. Biggs Company, 2255 Barry Avenue, West Los Angeles 64, California.

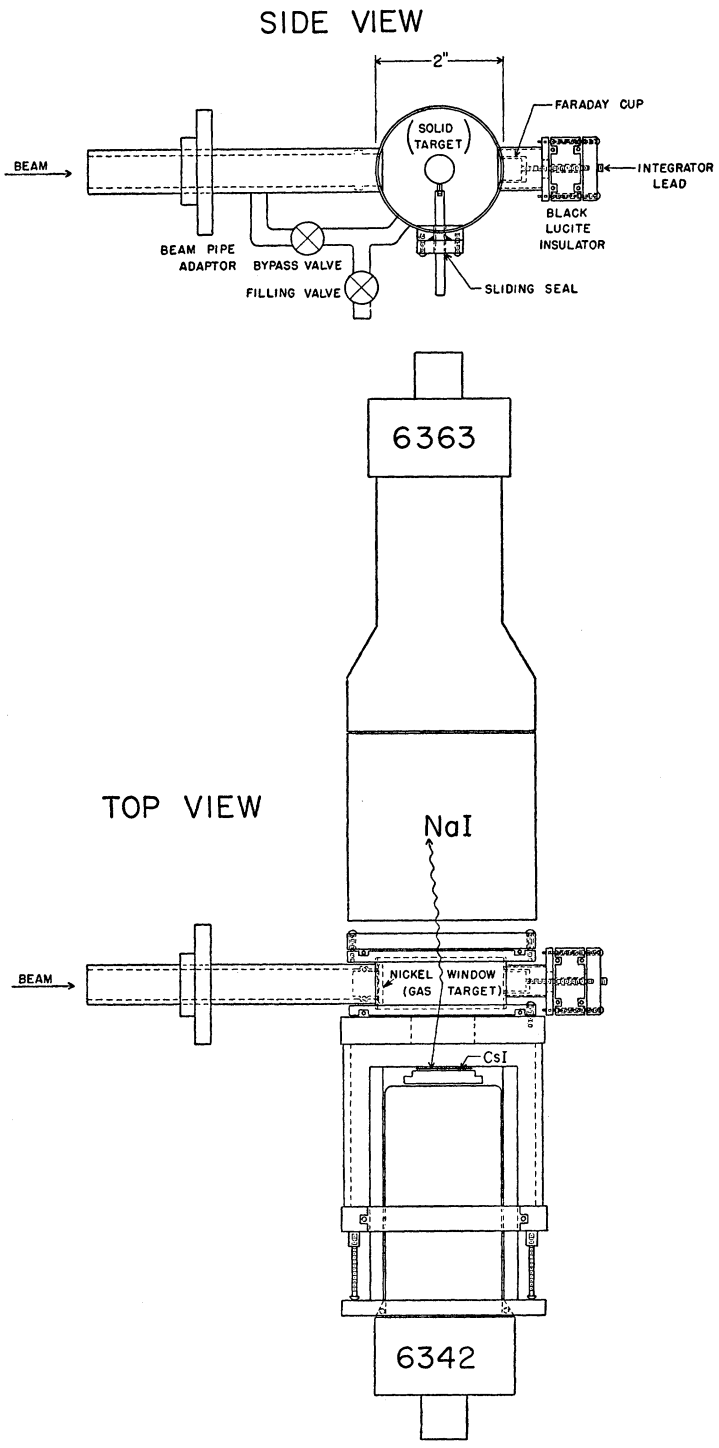

FIG. 4. Target chamber for charged particle-gamma ray coincidence measurements.

Particles scattered from the chamber, probably from the collector cup, were found to reach the unshielded CsI crystal. Detector shields of tantalum with circular apertures of 3/4 in. or less eliminated these particles. Shields having 1/8-in. or 1/4-in. slits aligned perpendicular to the beam served also to reduce the loss of resolution resulting from the dependence of the particle energy on the polar angle of scattering. The detector usually was employed with a 1/4-in. slit shield placed about an inch above the crystal.

The incident beam was defined by tantalum collimators with center holes 1/8 in. or 1/16 in. in diameter.

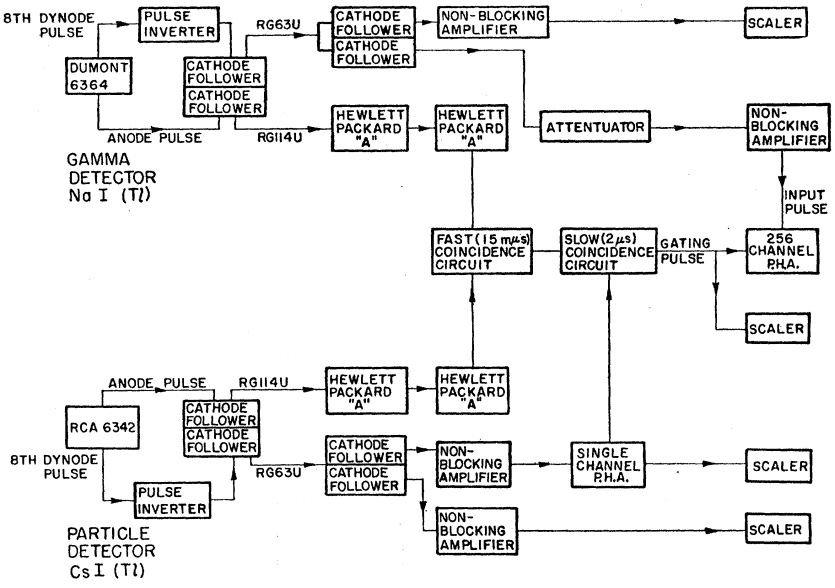

FIG. 5. Block diagram of the electronics used for charged particle-gamma coincidence measurements.

These were placed immediately before the adaptor tube. Beams were thus reduced to a few hundredths of a microampere or less, in order to obtain an acceptable true to accidental coincidence rate.

Tests using the annihilation quanta of a Na^{22} source showed that the detection efficiency of the Garwin fast coincidence circuit for the resolving time used was approximately constant only for pulses larger than 4 or 5 volts from the phototube anode. Since the pulses of interest might be only a small fraction of the size of those corresponding to other spectral peaks, the resulting anode spectrum under this requirement was very nonlinear and unsuitable for pulse-height analysis. Therefore, pulses for analysis were taken from the eighth dynode of the phototube.

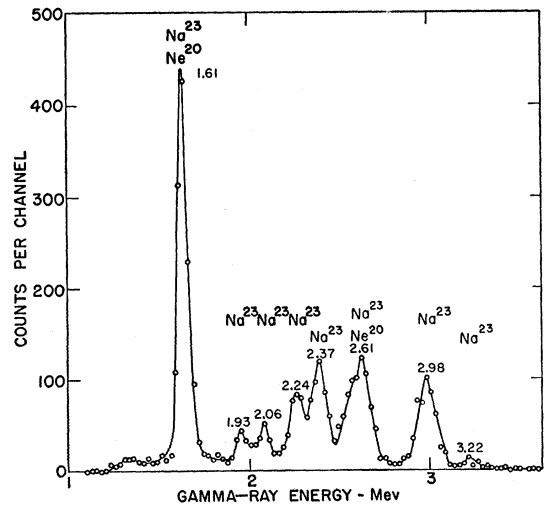

FIG. 6. Three-crystal pair spectrum of the gamma rays from bombardment of NaI with 4.68-Mev protons.

It was observed at high gain that photomultiplier pulses were reduced in size. This was attributed to a space charge effect in the latter stages. The increased voltage for the latter stages needed to overcome this effect was obtained by employing two independently variable supplies, one for the first eight stages of the photomultiplier and another for the remaining stages. The latter was a regulated supply, capable of furnishing the large currents required in the later stages at high gain and high counting rate. In addition, this arrangement permitted independent variation of the size of the pulses used for analysis and for fast coincidence.

The ratio of chance to true coincidences was usually less than 1 in 20, as determined by addition of an artificial delay in one input of the fast coincidence circuit. A block diagram of the detecting and analyzing electronics used for the particle-gamma coincidence measurements is shown in Fig. 5. (A fast Rossi-type coincidence circuit employing EFP60 tubes was used for the Ne+p coincidence spectrum shown in Fig. 27. This circuit was abandoned because of difficulties in-

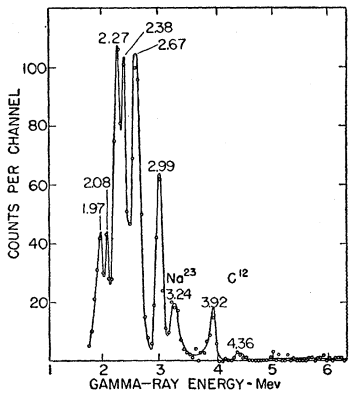

FIG. 7. Three-crystal pair spectrum of the gamma rays from bombardment of NaI with 5.0-Mev protons.

volving singles feed through, and the Garwin circuit used thereafter.)

4. Calibration Procedure

The gamma rays from Na^{22}, Co^{60}, and Cs^{137} sources were used for energy calibration. Intense reaction gamma rays of well-known energy, such as the 1.64-Mev gamma from Na^{23} and Ne^{20} or the 440-kev gamma from Na^{23}, were also used.

III. EXPERIMENTAL RESULTS

1. Three-Crystal Pair Spectrometer

Spectra were taken, with the three-crystal pair spectrometer, of gamma rays resulting from proton bombardment of thin evaporated Na and NaI targets at

TABLE I. Observed gamma rays and transition assignments for Na^{23} and Ne^{20} transitions.

E_γ (Mev)[a]	Transition[a] (Mev)	Method of observation[b]
		Na^{23}
0.44	0.44–0	s; $\gamma-\gamma_{1.6}$; $\gamma-p'$
0.62	2.70–2.08	s; $\gamma-\gamma_{0.44}$; $\gamma-\gamma_{1.6}$; $\gamma-p'$
1.64	2.08–0.44	s; $\gamma-\gamma_{0.44}$; $\gamma-p'$; 3-crystal
1.95	2.39–0.44	s; $\gamma-\gamma_{0.44}$; $\gamma-p'$; 3-crystal
2.08	2.08–0	s; $\gamma-p'$; 3-crystal
2.26	2.70–0.44	s; $\gamma-\gamma_{0.44}$; $\gamma-p'$; 3-crystal
2.39	2.39–0	s; $\gamma-p'$; 3-crystal
2.54	2.98–0.44	$\gamma-\gamma_{0.44}$; $\gamma-p'$
2.64	2.64–0	s; $\gamma-p'$; 3-crystal
2.98	2.98–0	s; $\gamma-p'$; 3-crystal
3.24	3.68–0.44	$\gamma-p'$; 3-crystal
3.92	3.92–0	$\gamma-p'$; 3-crystal
		Ne^{20}
1.64	1.64–0	s; $\gamma-p'$; $\gamma-\alpha$; 3-crystal
2.61	4.25–1.64	s; $\gamma-\gamma_{1.6}$; $\gamma-p'$; $\gamma-\alpha$; 3-crystal
3.33	4.97–1.64	$\gamma-\gamma_{0.6}$; $\gamma-\alpha$; 3-crystal

[a] Energy level values from the magnetic spectrograph measurements of W. W. Buechner and A. Sperduto, Phys. Rev. **106**, 1008 (1957).
[b] s = single crystal; 3-crystal = three-crystal pair spectrometer; $\gamma-\gamma_E$ = gammas coincident with gamma of energy E; $\gamma-p'$ and $\gamma-\alpha$ = gammas coincident with inelastically scattered protons and with alpha particles, respectively.

bombarding energies of 4.68, 5.0, 6.0, and 6.31 Mev. The spectrometer was placed at an angle of 90° with respect to the beam.

Figures 6 through 9 show the spectra obtained and the gamma-ray energies. A summary of the observed gamma rays and transition assignments is given in Table I. Average gamma-ray energies obtained in these four runs were 1.95±0.02, 2.09±0.02, 2.27±0.02, 2.39±0.02, 2.99±0.02, 3.93±0.03, and 4.42±0.04 Mev. Calibration was based on the singles peak position in the center crystal of the Na^{22} 0.511- and 1.28-Mev gammas. The 4.42-Mev gamma may arise from the 4.43 Mev to ground-state transition from either Na^{23} or from C^{12} contamination. The C^{12} assignment is more probable since other possible transitions from this state in Na^{23} are not observed, since in some spectra this gamma ray is very strong relative to those from more

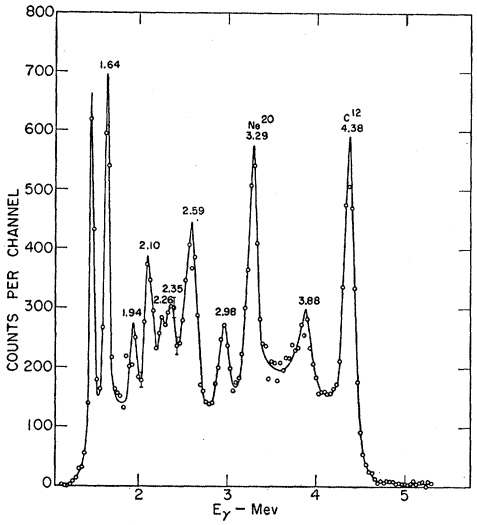

FIG. 8. Three-crystal pair spectrum of the gamma rays from bombardment of Na with 6.0-Mev protons.

easily populated lower lying Na^{23} levels, and since resonances for production of the 4.43-Mev gamma ray from C^{12} are known to occur at bombarding energies above 5 Mev. The gamma ray of about 2.64 Mev observed at all bombarding energies is believed to arise both from the Na^{23} transition between the 2.64 Mev and the ground state and from the Ne^{20} transition between the 4.25- and 1.64-Mev states. The average energy of all such gamma rays is 2.64±0.02. On the basis of a rough preliminary examination of the energy dependence of charged particle yields, the yield of alphas to the 4.25-Mev state of Ne^{20} is expected to be small at the lowest bombarding energy, E_p=4.68. The

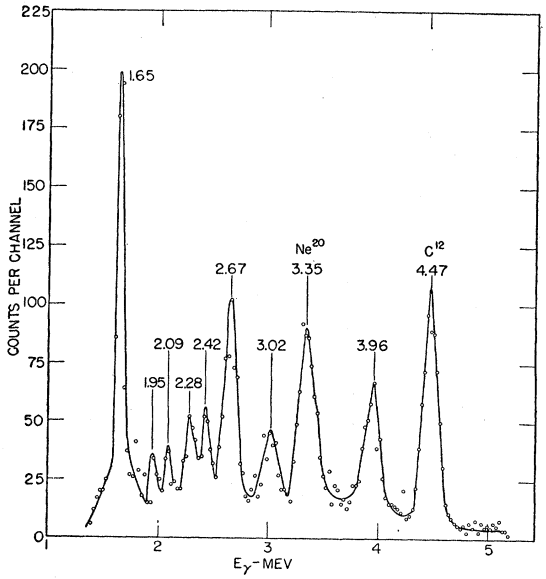

FIG. 9. Three-crystal pair spectrum of the gamma rays from bombardment of Na with 6.31-Mev protons.

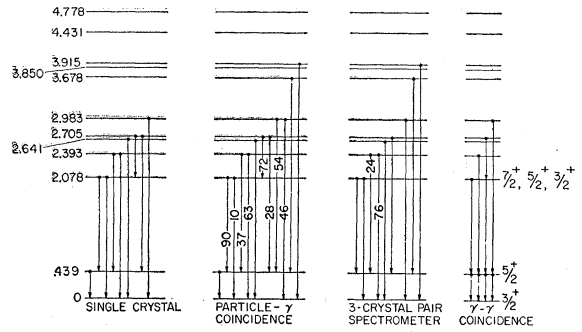

FIG. 10. Level diagram and gamma-ray decay scheme of Na^{23}.

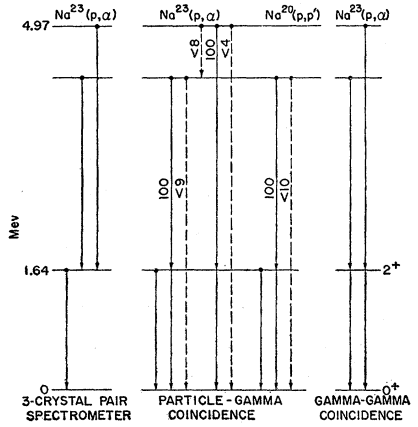

FIG. 11. Level diagram and gamma-ray decay scheme of Ne^{20}. *Note.*—The notation at the top of the Figure "$Na^{20}(p,p')$" should read "$Ne(p,p')$."

Na^{23} transition between the 2.64 Mev and ground states has been observed from inelastic neutron scattering[9] and from proton capture by Ne^{22}.[10]

The Ne^{20} transition between the 4.25- and 1.64-Mev states is known to occur from the gamma-gamma and particle-gamma coincidence measurements described later. The gamma rays of about 3.23 Mev observed at $E_p=4.68$ and 5.0 are attributed to the Na^{23} transition between the states at 3.68 and 0.44 Mev. At $E_p=6.0$ and 6.31, the gamma ray of about 3.3 Mev is believed to represent mainly the Ne^{20} transition between the states at 4.97 and 1.64 Mev. Such a transition was observed also in gamma-gamma and particle-gamma coincidence spectra; on the basis of the particle excitation behavior, the alpha group to the 4.97-Mev state of Ne^{20} is not expected to appear at the lower energies. The strong gamma ray of 1.64 Mev appearing at all bombarding energies is attributed both to the Na^{23} transition between the 2.08- and 0.44-Mev states and to the Ne^{20} transition between the 1.64 and ground states. The apparent strong gamma ray of about 1.4 Mev shown in Fig. 8 is believed to be merely an instrumental effect. Figures 10 and 11 show the Na^{23} and Ne^{20} level schemes, the observed low-energy gamma-ray transitions, and the calculated relative decay probabilities.

High-energy gamma rays from the $F^{19}(d,n\gamma)Ne^{20}$ reaction were observed using the three-crystal pair spectrometer. Figure 12 shows the spectrum obtained from the bombardment of a BaF_2 target with 80 microcoulombs of 3.35-Mev deuterons. Figure 13 is a similar spectrum showing only the high-energy gamma rays. These spectra were calibrated using the 6.14- and 7.01-Mev (6.91 and 7.12 unresolved) peaks from the $F^{19}(p,\alpha\gamma)O^{16}$ reaction. The gamma-ray energies obtained from these results are listed and compared with other experiments in Table II. Similar spectra taken at a deuteron bombarding energy of 5.52 Mev showed no additional gamma rays. No gamma rays with energies greater than 11.5 Mev were observed from the $F^{19}+d$ reaction.

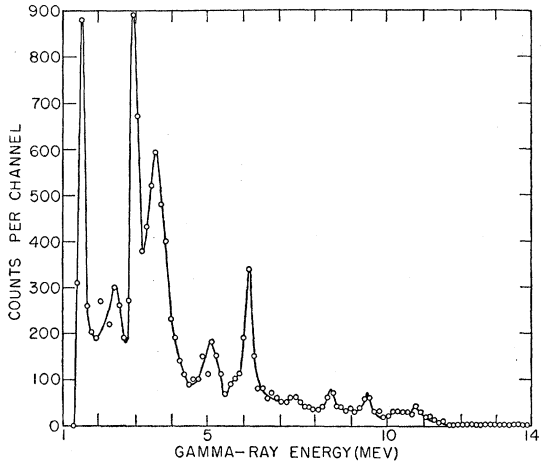

FIG. 12. Three-crystal pair spectrum of the gamma rays from the bombardment of a BaF_2 target with 3.35-Mev deuterons.

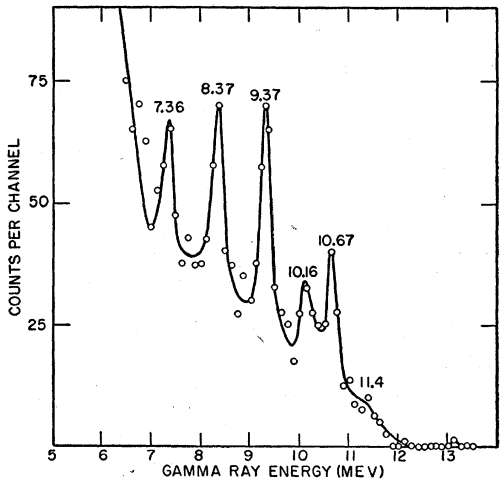

FIG. 13. Three-crystal pair spectrum of the high-energy gamma rays from the bombardment of a BaF_2 target with 3.35-Mev deuterons.

[9] J. M. Freeman and J. H. Montagu, Nuclear Phys. **9**, 181 (1958/59).

[10] J. J. Singh, V. W. Davis, and R. W. Krone, Phys. Rev. **115**, 170 (1959).

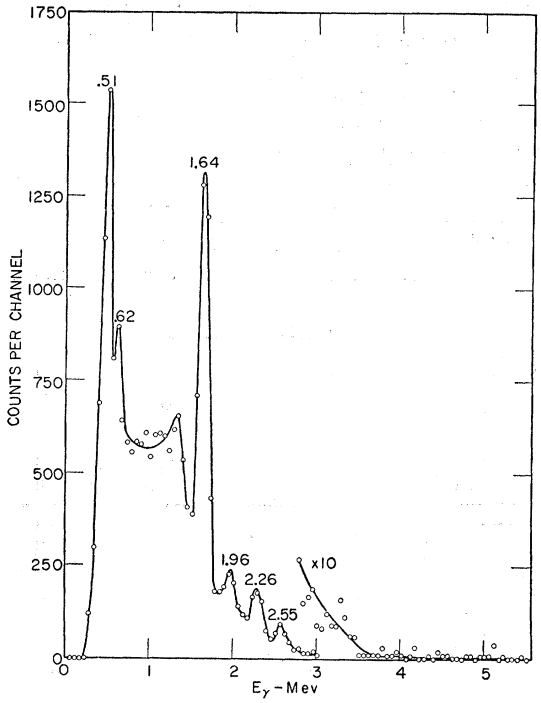

FIG. 14. Gamma-ray spectrum coincident with the 440-kev gamma ray of Na^{23}. NaI+p, E_p=5.15 Mev.

TABLE II. Gamma rays from F^{19}+d.

Gamma-ray energies[a] (Mev)			
Present results	Bent *et al.*[b]	Terrell *et al.*[c]	Assignment
11.4 ±0.1	11.56±0.19	11.5±0.4	Ne^{20}
10.67±0.05	10.65±0.09		Ne^{20}
10.16±0.05	10.01±0.09		Ne^{20}
9.37±0.05	9.38±0.09	9.3±0.3	Ne^{20}
8.37±0.05		8.1±0.4	Ne^{20}
7.36±0.05			Ne^{20}
6.14±0.05			Ne^{20}, F^{20}, or O^{16}
5.14±0.07			Ne^{20} or F^{20}
3.63±0.07			Ne^{20}, F^{20}, or O^{17}
3.02±0.05			Ne^{20}, F^{20}, or O^{17}
2.52±0.05			Ne^{20}, F^{20}, or O^{17}

[a] Uncorrected for possible Doppler shifts (see reference b).
[b] R. D. Bent, T. W. Bonner, J. H. McCrary, W. A. Ranken, and R. F. Sippel, Phys. Rev. **99**, 710 (1955).
[c] J. Terrell and G. C. Phillips, Phys. Rev. **83**, 703 (1951).

The 11.4-, 10.67-, 10.16-, 9.37-, and 8.37-Mev gamma-ray energies agree with earlier experiments within the experimental errors. The lower energy gamma rays have not been previously reported.

The four highest energy gamma rays are assigned to Ne^{20} (see reference *b* of Table II). The 8.37- and 7.36-Mev gamma rays are also assigned to Ne^{20} and may be due to ground-state transitions from states in Ne^{20} at these energies, or to cascade transitions involving higher energy states. Definite assignments for the lower energy gamma rays cannot be made because bound final states following the (d,p), $(d,n\alpha)$ and (d,α) reactions can give gamma rays in this energy range.

2. Gamma-Gamma Coincidence Measurements

Spectra were obtained, from the proton bombardment of Na at various energies, of gamma rays in coincidence with the 440-kev gamma of Na^{23} and with the 1.6-Mev gamma rays arising both from the Na^{23} transition between the 2.08- and 0.44-Mev states and from the Ne^{20} transition between the 1.64-Mev and ground states. Some of these spectra are shown in Figs. 14 through 18. Table I summarizes the observed gamma rays and transition assignments. The 0.5-Mev gamma of Figs. 14 and 15 is attributed to the annihilation quanta of the positron activity following the $Na^{23}(p,n)$-Mg^{23} reaction (Q=−4.84 Mev), since the tail of the 511-kev annihilation quantum spectrum fell within the window set on the 440-kev gamma. The 3.45-Mev γ of Fig. 15 may represent a cascade through the 0.44-Mev state from either the 3.85- or 3.92-Mev states. The 3.85 → 0.44-Mev cascade has been observed from the $Ne^{22}(p,\gamma)$ reaction.[10]

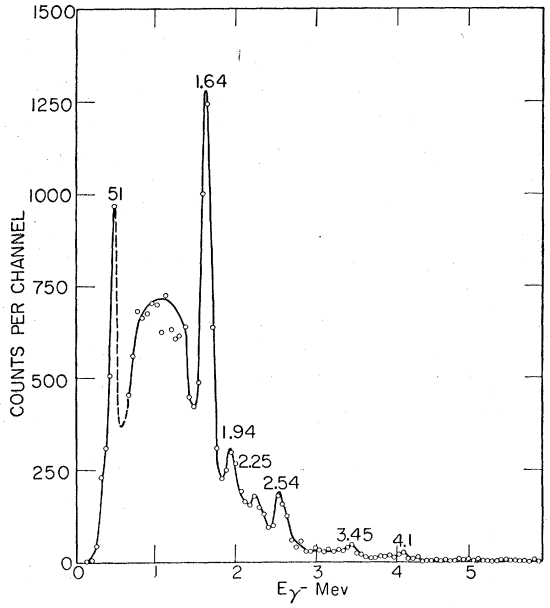

FIG. 15. Gamma-ray spectrum coincident with the 440-kev gamma ray of Na^{23}. Na+p, E_p=5.43 Mev.

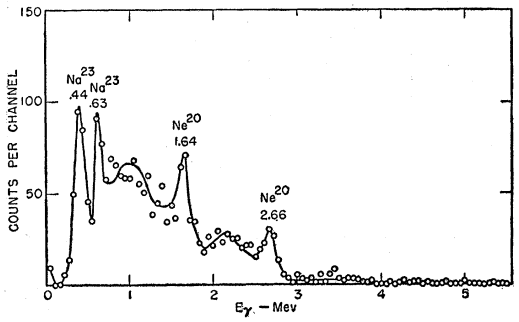

FIG. 16. Gamma-ray spectrum coincident with the 1.6-Mev gamma rays of Na^{23} and Ne^{20}. NaI+p, E_p=5.15 Mev.

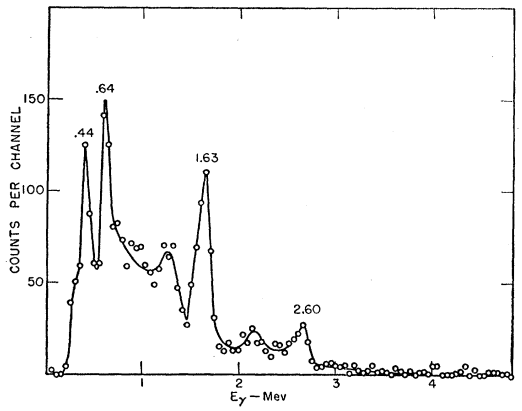

FIG. 17. Gamma-ray spectrum coincident with the 1.6-Mev gamma rays of Na^{23} and Ne^{20}. NaI+p, E_p=4.55 Mev.

The gamma spectrum in coincidence with 1.6-Mev gamma rays at E_p=5.15 Mev (Fig. 16) shows a fairly strong gamma of 0.63 Mev, which might be assigned to a Na^{23} transition between the states at 2.70 and 2.08 Mev. A definite strong 0.64-Mev gamma appears also in coincidence with the 1.6-Mev gamma at E_p=4.55 Mev (Fig. 17). It is unlikely that this peak could represent a Na^{23} transition between the states of 2.64 and 2.08 Mev. This gamma (0.63 Mev) does not appear strongly in coincidence with the 1.6-Mev gamma at bombarding energies of 5.00, 5.43, and 5.45 Mev. An unassigned gamma ray of 0.650 Mev has been observed from inelastic scattering of neutrons from Na^{23}.[11]

Since the Na^{23} 2.08-Mev state has a strong cascade branch through the 0.44-Mev state, any transition between the 2.70- and 2.08-Mev states should appear also in coincidence with 0.44-Mev gammas. The expected 0.62-Mev peak is largely masked by the annihilation quanta peak due to the choice of 180° for the relative detector location, although there is a weak 0.62-Mev peak in Fig. 14.

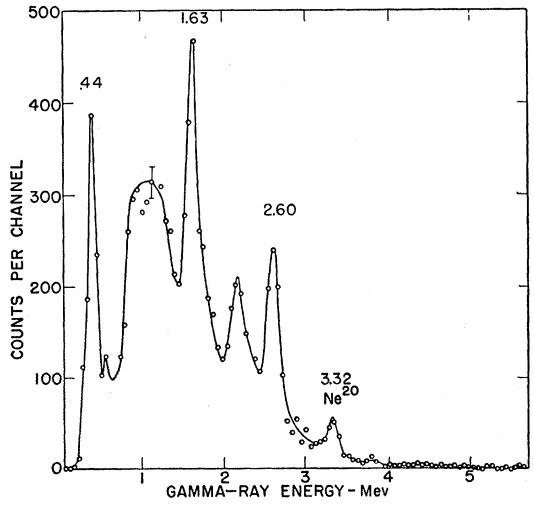

FIG. 18. Gamma-ray spectrum coincident with the 1.6-Mev gamma rays of Na^{23} and Ne^{20}. NaI+p, E_p=5.43 Mev.

[11] I. L. Morgan, Phys. Rev. **103**, 1031 (1956).

Spectra in coincidence with 1.6-Mev gammas at bombarding energies of 4.55, 5.00, 5.15, and 5.45 Mev exhibit peaks at about 2.6, 2.1, 1.6, and 0.44 Mev. The 2.6- and 2.1-Mev peaks represent the full energy loss and one escape peak of the Ne^{20} transition between the states at 4.25 and 1.64 Mev. The strong 1.6-Mev peaks represent the two escape peaks of the Ne^{20} 2.6-Mev gamma-ray transition and also coincidences between the Ne^{20} 1.64-Mev gamma transition and that part of the 2.6-Mev gamma tail which falls within the single-channel analyzer window. In addition, the spectrum obtained with E_p=5.43 Mev (Fig. 18) shows a weak but definite peak at about 3.3 Mev in coincidence with 1.6-Mev gammas, which is attributed to the transition between the Ne^{20} states at 4.97 and 1.64 Mev.

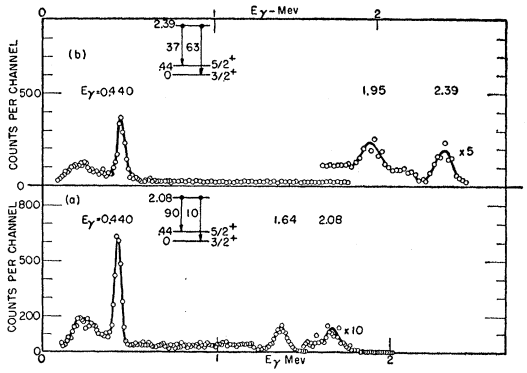

FIG. 19. (a) Gamma-ray spectrum coincident with protons inelastically scattered to the 2.08-Mev state of Na^{23}. NaI+p, E_p=4.01 Mev. (b) Gamma-ray coincident with protons inelastically scattered to the 2.39-Mev state of Na^{23}. NaI+p, E_p=4.24 Mev. [The energy scale for Fig. 19(a) is incorrect.]

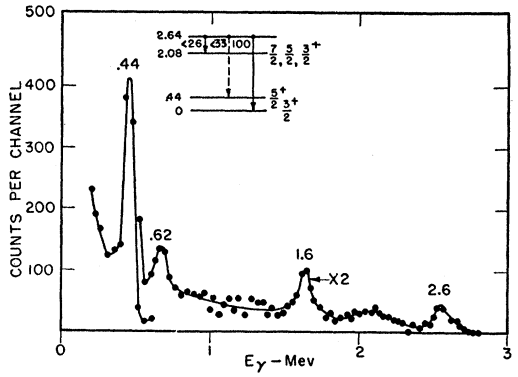

FIG. 20. Gamma-ray spectrum coincident with protons inelastically scattered to the 2.64-Mev state of Na^{23}. NaI+p, E_p=4.08 Mev.

An attempt was made to measure the correlation of the 2.6- and 1.6-Mev gammas in the cascade decay of

the Ne^{20} 4.25-Mev state. The state was populated by the p,α reaction from bombardment of a thick evaporated target of NaI. The bombarding energy chosen, 5.08 Mev, was expected to yield very few 3.3–1.6 Mev gamma-ray coincidences from the Ne^{20} cascade transitions among the states $4.97 \rightarrow 1.64 \rightarrow 0$ Mev. This expectation was confirmed by a preliminary coincidence spectrum taken in close geometry.

The fixed 3 in.×2 in. NaI(Tl) detector output was channeled on the photopeak of the 1.6-Mev gamma,

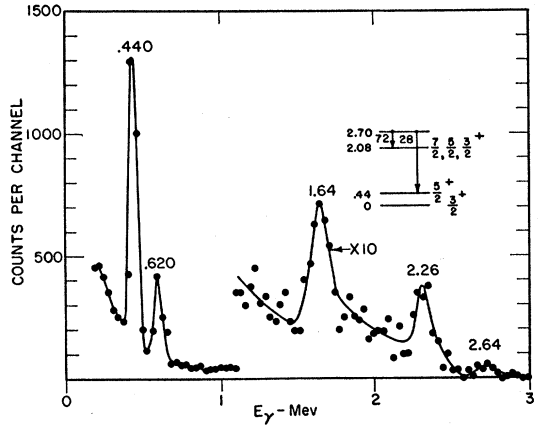

FIG. 21. Gamma-ray spectrum coincident with protons inelastically scattered to the 2.70-Mev state of Na^{23}. NaI+p, E_p=5.11 Mev.

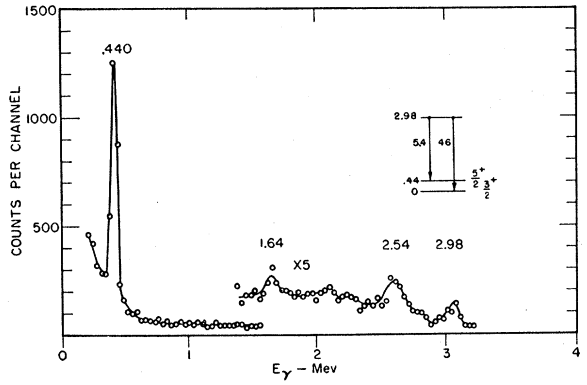

FIG. 22. Gamma-ray spectrum coincident with protons inelastically scattered to the 2.98-Mev state of Na^{23}. NaI+p, E_p=4.68 Mev.

the 3 in.×3 in. NaI(Tl) detector was placed successively at 90° and at 180° relative to the fixed counter. The crystal faces were about $2\frac{3}{4}$ in. from the target. Coincidence counts were normalized by monitoring the fixed counter.

It was hoped that an isotropic population of the 4.2-Mev state would result from averaging over compound nuclear levels, because of the thickness of the target. To test this hypothesis, the correlation was was measured with the fixed counter oriented at 90°

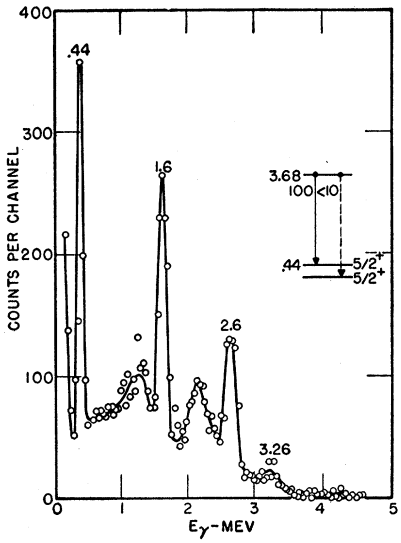

FIG. 23. Gamma-ray spectrum coincident with protons inelastically scattered to the 3.68-Mev state of Na^{23}. NaI+p, E_p=5.6 Mev.

and at 135° with respect to the incident beam. The anisotropy reversed its sense. With the fixed counter at 90° the ratio of coincidence counts for 90° to those for 180° relative angle was 1.22±0.06, whereas with the fixed counter at 135° this ratio was 0.85±0.07. Such a result is inconsistent with zero spin for the 4.2-Mev state.

3. Particle-Gamma Coincidence Measurements

After preliminary excitation curves were taken for identification of the particle groups, spectra were taken at appropriate energies of gamma rays in coincidence with various charged particle groups. These spectra are shown in Figs. 19 through 27. A summary of the observed gamma rays and transition assignments is given in Table I.

The 0.60-, 1.64-, and 0.44-Mev gammas of Fig. 20 probably represent the cascade transitions among the

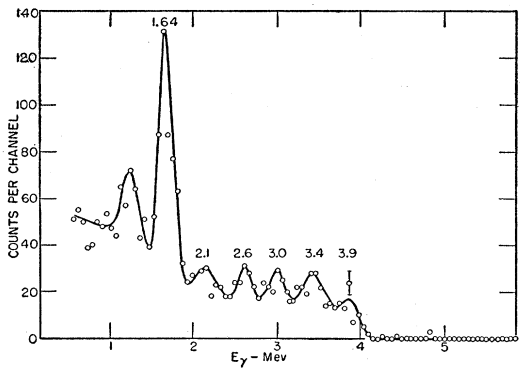

FIG. 24. Gamma-ray spectrum coincident with protons inelastically scattered to the 3.92-Mev state of Na^{23}. NaI+p, E_p=5.83 Mev.

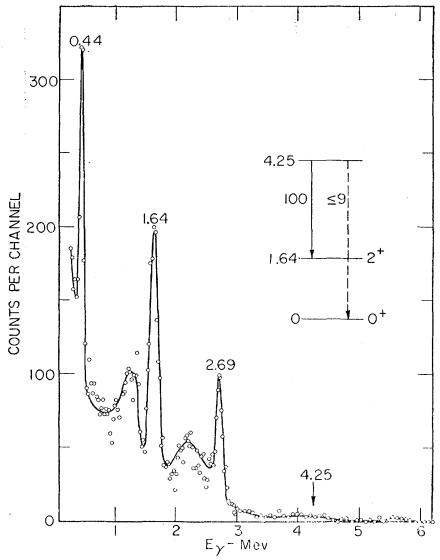

FIG. 25. Gamma-ray spectrum coincident with alpha particles to the 4.25-Mev state of Ne^{20}. NaI+p, E_p=5.47 Mev.

Na^{23} states 2.70 → 2.08 → 0.44 → 0 Mev, arising from true coincidences with protons inelastically scattered to the 2.70-Mev state of Na^{23}, which fell within the single-channel analyzer "window." At this bombarding energy the alpha group to the 4.25-Mev state of Ne^{20} would lie close to the "window"; this state is known from gamma-gamma coincidence measurements to decay mainly by cascade giving rise to 2.6- and 1.6-Mev gamma rays. It is expected, however, on the basis of the particle excitation runs, that the yield of this alpha group would be small at this bombarding energy.

The peak near 2.7 Mev in Fig. 21 is attributed to the Na^{23} transition between the 2.64-Mev and ground states, arising from protons inelastically scattered to the 2.64-Mev state which fell within the single-channel analyzer "window." The 2.3- and 0.44-Mev peaks are attributed to the cascade decay among the Na^{23} states 2.70 → 0.44 → 0 Mev, consistent with the three-crystal observation of a gamma ray of average energy 2.27 Mev. The 0.6-, 1.6-, and 0.44-Mev peaks are attributed to the cascade decay among the Na^{23} states 2.70 → 2.08 →0.44 → 0 Mev. Population of the 2.08-Mev state by cascade should lead to a 2.08 Mev → ground-state transition; however, this is a weak branch and is not observed. The large difference in the ratio of the heights of the 2.7- and 0.6-Mev peaks between Figs. 20 and 21 supports the assumption that they originate mainly from different states. The assignment made for the 2.7-Mev gamma is also consistent with the absence of any three-crystal pair spectrometer evidence for a ground-state transition from the 2.70-Mev state of Na^{23}. Results from inelastic neutron scattering on Na^{23} [9] and from proton capture in Ne^{22} [10] agree with these assignments.

The 2.6- and 1.6-Mev gammas of Fig. 23 are attributed to Ne^{20} cascade transitions among the states 4.25 → 1.64 → 0 Mev, arising from coincidences with the alpha group to the 4.25-Mev state of Ne^{20} which fell within the single-channel analyzer "window." There is no evidence for any Na^{23} cascade among the states 3.68 → 2.08 → 0.44 → 0 Mev. The corrected strength of the 2.6-Mev gamma-ray peak agrees well with that of the 1.6-Mev gammas, suggesting that both arise entirely from the Ne^{20} cascade. Similarly, the corrected strength of the 3.2-Mev gamma peak agrees well with that of the 0.44-Mev peak, suggesting that the 3.68-Mev state feeds the 0.44-Mev state of Na^{23} only by a direct 3.2-Mev cascade gamma ray.

Several of the peaks of Fig. 24 may represent coincidences with the alpha groups to the 4.2- and 4.9-Mev Ne^{20} states, which fell close to the "window" at this bombarding energy.

(The proton groups to the 3.92- and 3.85-Mev states of Na^{23} could not be resolved. Therefore, the interpretation of the spectrum of Fig. 24 as a ground-state transition arising from the 3.92-Mev state rather than from the 3.85-Mev state, is based on the average energy of 3.93±0.03 Mev obtained from the three-crystal pair spectrometer spectra. This interpretation is consistent with the results of Singh *et al.*[10])

The 0.44-Mev gamma ray of Fig. 25 is attributed to the Na^{23} transition between the ground and first excited states, and is probably due to true coincidences with protons inelastically scattered to the 3.68-Mev state, which cascades through the 0.44-Mev state, with the 3.24-Mev cascade gamma spectrum being too dispersed to observe.

The gamma spectrum coincident with the alpha group to the 4.9-Mev state of Ne^{20} (Fig. 26, E_p=5.82 Mev) shows gamma rays of 3.3 and 1.6 Mev, and a cutoff at about 5.0 Mev. The 3.3- and 1.6-Mev gammas are attributed to the Ne^{20} cascade transition among the states 4.97 → 1.64 → 0 Mev. Two small peaks are observed, at 4.9 and 4.6 Mev, which resemble the full energy loss and one escape peaks of a ground-state

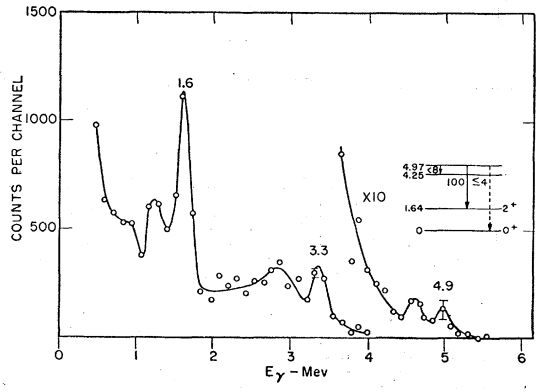

FIG. 26. Gamma-ray spectrum coincident with alpha particles to the 4.97-Mev state of Ne^{20}. NaI+p, E_p=5.82 Mev.

transition from the 4.97-Mev state. However, at least part of these counts represent simultaneous detection of the 1.6- and 3.3-Mev cascade gammas in the crystal.

A spectrum was obtained in an early run, by proton bombardment of natural neon, of the gammas in coincidence with protons inelastically scattered to the 4.25-Mev state of Ne^{20} (Fig. 27). (A Rossi-type EFP60 fast coincidence circuit was used for this spectrum only.) This spectrum shows gamma rays of 2.7 and 1.6 Mev, attributed to the cascade transition among the Ne^{20} states $4.25 \rightarrow 1.64 \rightarrow 0$ Mev. No inelastic proton group corresponding to the 4.97-Mev state of Ne^{20} was observed for bombarding energies up to 6.5 Mev. The 2.4-Mev gamma ray and part of the 1.6-Mev gamma are attributed to the cascade decay among the N^{14} states $3.95 \rightarrow 2.31 \rightarrow 0$ Mev, and result from gamma coincidences with protons inelastically scattered to the 3.95-Mev state. The presence of N^{14} in the target gas was undoubtedly due to air contamination during filling. The gamma peak at 1.3 Mev and part of the peak at 2.1 Mev are attributed to the Ne^{22} cascade decay among the states $3.35 \rightarrow 1.28 \rightarrow 0$ Mev. (The low-energy gamma tail was biased out in the fast coincidence circuit in order to prevent singles feed through.) These gammas are believed to represent true coincidences with protons inelastically scattered to the 3.35-Mev state of Ne^{22}. The presence of this proton group within the single-channel analyzer "window" set for the proton group to the 4.2-Mev state of Ne^{20} is probably due to an instability observed to occur in the amplifier at high counting rates. This instability consisted of a base line fluctuation of several volts which was caused by a very long negative undershoot following the positive output pulse. This fluctuation was subsequently eliminated by modification of the amplifier to perform only one differentiation with short time constant at the amplifier output where, previously, two differentiations had been performed, by a short time constant element at an intermediate point and a medium time constant output element.

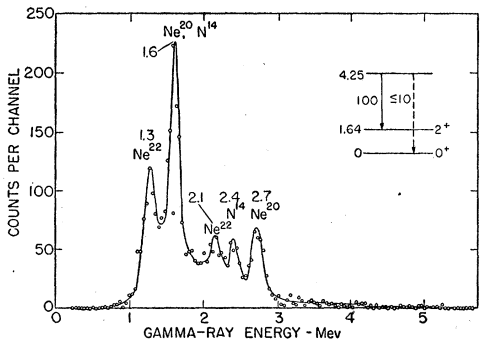

FIG. 27. Gamma-ray spectrum coincident with protons inelastically scattered to the 4.25-Mev state of Ne^{20}. Ne+p, E_p=5.85 Mev.

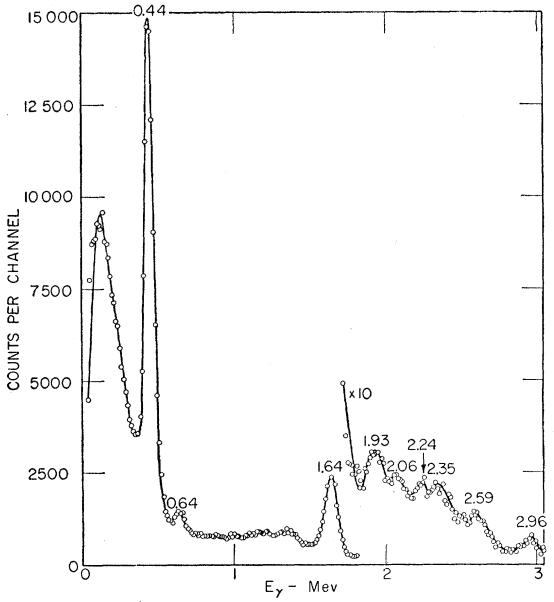

FIG. 28. Single-crystal gamma-ray spectrum from the bombardment of NaI with 5.20-Mev protons.

4. Single-Crystal Gamma-Ray Spectra

Many gamma spectra were obtained at various energies using a single large NaI crystal. A summary of the gamma rays so observed is shown in Fig. 10. Many of the gammas observed by other methods were seen also in the singles spectra. In particular, a gamma ray of about 0.6 Mev was readily observed at several bombarding energies. One such spectrum is shown in Fig. 28. A spectrum was taken at high gain at a bombarding energy of 4.88 Mev to obtain an accurate energy determination for this gamma. The value obtained was 0.631 ± 0.010 Mev, consistent with the assignment of this gamma ray to the Na^{23} transition between the states of 2.70 and 2.08 Mev.

IV. ANALYSIS OF EXPERIMENTAL DATA

1. Branching Ratios from Three-Crystal Data

The various gamma spectra obtained were analyzed to determine branching ratios. A summary of the results is shown in Figs. 10 and 11 and in Table III.

The extraction of such information from three-crystal spectra is severely limited in this instance by the inability of this technique to detect gamma rays of energy less than the pair-production threshold, and by the frequent occurrence of transitions of approximately equal energy in both Na^{23} and Ne^{20}. In a few cases, branching ratios could be calculated and in others upper limits could be estimated for unobserved transitions.

These branching ratios were based on the area of the well-defined two escape "peak triangle" after subtraction of the tails of higher energy gammas. A cor-

TABLE III. Observed gamma-ray branching ratios of excited states of Na^{23} and Ne^{20}.

Level (Mev)	Observed branching ratios	Method of Observation
	Na^{23}	
2.08	$2.08/1.64=0.11\pm0.03$	$p'-\gamma$
2.39	$2.39/1.95=1.7\pm0.3$	$p'-\gamma$
	$2.39/1.95=3.1$	3-crystal
	$2.39/0.31\geq3.5$	$p'-\gamma$
2.64	$2.64/2.20\geq4$	$p'-\gamma$
	$2.64/0.56\geq3$	$p'-\gamma$
2.70	$2.26/0.62=0.31\pm0.08$	$p'-\gamma$
	$2.79/0.62\leq0.15$	$p'-\gamma$
2.98	$2.98/2.54=0.84\pm0.17$	$p'-\gamma$
3.68	$3.68/3.24\leq0.10$	$p'-\gamma$
	$3.68/3.24\leq0.25$	3-crystal
3.85	No transitions observed	
3.92	$3.92/3.48\geq2.5$	$p'-\gamma$
	$3.92/3.48\geq2.0$	3-crystal
	Ne^{20}	
4.25	$4.25/2.61\leq0.10$	$\alpha-\gamma$
	$4.25/2.61\leq0.11$	$p'-\gamma$
4.97	$4.97/3.33\leq0.04$	$\alpha-\gamma$
	$0.72/3.33\leq0.08$	$\alpha-\gamma$

rection factor was applied for the high- and low-energy tails, based on the spectral shapes of several isolated gamma rays. The total number of spectral counts thus obtained for each peak was corrected for the iodine pair-production cross section and the branching ratio computed, neglecting possible angular distribution effects.

2. Branching Ratios from Particle-Gamma Data

For the particle-gamma spectra, the total number of counts in the spectrum of each observed gamma peak was obtained from the number in the full energy loss peak by using the curves of Heath.[12] Corrections to gamma-ray peaks for the tails of higher energy gamma rays were made from standard gamma-ray spectral shapes. A correction was made to the observed full energy loss peak counts for transmission through approximately 3/8 in. Al of the chamber cover plate and crystal light shield. Full energy loss peak counts were then determined by straight-line extrapolation of the sides of well-defined peaks to the base line or, for poorly defined peaks, by counting an appropriate energy width around the peak as determined from the standard spectral shapes. These standard shapes were taken from Heath's catalog; in addition, a 4.43-Mev gamma spectrum obtained from $C^{12}+p$ bombardment was used. The total number of spectral counts thus obtained for each gamma ray was corrected for the detection efficiency of the 3 in.$\times$3 in. crystal as given by Heath, and the observed branching ratios computed for the transition assignments previously given. Corrections were applied for the simultaneous detection of cascade gammas with resulting "sum peak" counts, assuming an isotropic angular correlation.

[12] R. L. Heath, Atomic Energy Commission Research and Development Report IDO-16408, 1957 (unpublished).

Curve fitting to a corrected gamma-ray spectrum was rejected as being unwarranted by the over-all precision of the computed branching ratios. The uncertainties stated in Table III include the statistical uncertainties both in the peak being analyzed and in those contributing background "tail" corrections, and also an estimate of the uncertainty in the tail correction factor.

Several of the gamma-particle coincidence spectra showed an appreciable excess of corrected 0.44-Mev Na^{23} gamma counts over the number of corrected counts for other members of the cascade. Angular correlation effects might explain some of the discrepancies; however, since the effect was sometimes quite large (a factor of two to four) and always in the same direction, it is believed that it is probably an instrumental effect. A possible explanation is that these represented true coincidences of gamma rays with particles which ordinarily would give pulses too big to pass through the window but which happened, by chance, to occur at the proper time after one of the very strong group of elastic pulses to be depressed in pulse height by the negative undershoot which followed the positive output pulses of the amplifier. A rough calculation of the expected frequency of this effect is in agreement with its observed magnitude.

The 0.44-Mev peak counts are therefore considered unreliable and have not been used in computing the branching ratios stated. The triple cascade among the Na^{23} states $2.70\rightarrow2.08\rightarrow0.44\rightarrow0$ Mev supports this assumption; the corrected strengths of the 0.63- and the 1.6-Mev gammas agree well, but there is a substantial excess of 440-kev gamma-ray counts above that expected from the strengths of the various feeding gammas. The corrected 440-kev counts are in good agreement with other cascade members for the transitions from the 2.08- and 3.68-Mev states, however.

In the gamma spectrum in coincidence with the alpha group to the 4.97-Mev state of Ne^{20} (Fig. 26), the total number of counts, corrected for chance coincidences, under the two small high-energy peaks is statistically significant although the shape of the peaks is not well defined. The chance correction was based on a coincidence spectrum taken under identical conditions as the spectrum of Fig. 26, but with a long piece of signal cable in one input of the fast coincidence circuit to mismatch the delays. The chance correction was a few percent.

The calculated correction for the "sum peak" of the 1.6- and 3.3-Mev gammas accounts for one-third to one-half of the total of approximately thirty counts under the full energy loss peak, assuming an angular correlation of the form $(1+\cos^2\theta)$. It is possible that the apparent residual effect represents statistical fluctuations in the sum peak and uncertainties of analysis. Therefore, a ground-state transition is not considered to be established and only an upper limit of 4% is set for it.

TABLE IV. Theoretical gamma-ray transition widths for excited states of Na^{23} and Ne^{20}, calculated from single-particle and collective models.

Level (Mev)	E_γ (Mev)	Observed branching ratio (crossover/cascade)	Single-particle widths $\Gamma_w(E1)$ (ev)	$\Gamma_w(M1)$ (ev)	$\Gamma_w(E2)$ (ev)	Collective model widths $\Gamma(M1)$ (ev)	$\Gamma(E2)$ (ev)	Spin-parity assumption
				Na^{23}				
0.44	0.44			1.8×10^{-3}	1.3×10^{-7}	5.9×10^{-4}	1.7×10^{-6}	
2.08	2.08	0.11 ± 0.03	7.9	0.19	3.1×10^{-4}		1.7×10^{-3}	$7/2^+$
	1.64		3.9	0.09	9.5×10^{-5}	4.5×10^{-3}	7.8×10^{-4}	
2.39	2.39	1.7 ± 0.3	12.1	0.28	6.2×10^{-4}			
	1.95		6.6	0.16	2.3×10^{-4}			
2.64	2.64	≥4	16.3	0.39	1.0×10^{-3}			
	2.20		9.5	0.22	4.1×10^{-4}			
2.70	2.26	0.31 ± 0.08	10.2	0.24	4.7×10^{-4}		3.9×10^{-3}	$9/2^+$
	0.62		0.21	0.005	7.3×10^{-7}	2.73×10^{-4}	4.1×10^{-6}	
2.98	2.98	0.84 ± 0.17	23.5	0.55	1.9×10^{-3}			
	2.54		14.5	0.34	8.4×10^{-4}			
3.68	3.68	≤0.10	44.2	1.0	5.3×10^{-3}			
	3.24		30.1	0.7	2.8×10^{-3}			
3.92	3.92	≥2.5	53.5	1.3	7.3×10^{-3}			
	3.48		37.4	0.88	4.1×10^{-3}			
				Ne^{20}				
1.64	1.64		3.6	0.09	6.5×10^{-5}			
4.25	4.25	≤0.09	61.5	1.6	8.9×10^{-3}			
	2.61		14.3	0.37	7.9×10^{-4}			
4.97	4.97	≤0.04	99.0	2.6	1.9×10^{-2}			
	3.33		30.0	0.77	2.6×10^{-3}			

A chance coincidence spectrum was taken of the gamma rays in coincidence with the alpha group to the 4.2-Mev state of Ne^{20} from proton bombardment of NaI (Fig. 25). Some of the scattered counts in the region of 4.2 Mev in these spectra may be due to true coincidences with protons inelastically scattered from the 4.43-Mev state of C^{12}. No peaks are observed; therefore, only an upper limit of 9% is placed on the ground-state branch from the 4.25-Mev state of Ne^{20} from these data. A limit of 10% is set for this branch from the spectrum of gammas in coincidence with protons inelastically scattered to the 4.2-Mev state of Ne^{20}, using a target of natural neon (Fig. 27).

V. DISCUSSION OF RESULTS

1. Spin and Parity Assignments

The spin and parity of the Na^{23} ground and first excited states are $3/2^+$ and $5/2^+$, respectively.[13] Allowed beta decay has been observed from Ne^{23} to the ground state and to the first two excited states of Na^{23}.[14] Therefore, the ground-state spin of Ne^{23} is $3/2^+$ or $5/2^+$ and the spin of the 2.08-Mev state of Na^{23} must be $3/2^+$, $5/2^+$, or $7/2^+$. Positive parity assignments have been made to the 2.08-Mev second excited state of Na^{23} and also to the 2.70- and 3.85-Mev states from inelastic deuteron scattering.[15]

Table IV lists the observed branching ratios and the transition widths, calculated from the Weisskopf single-particle expression and from the strong coupling collective model for the indicated spin assumptions, using the Nilsson eigenfunctions for $\Omega=3/2$, $N=2$. The expressions given by Wilkinson[16] were used in computing the single-particle widths; the expressions of Nilsson[17] and the modified $E2$ expression due to McManus and Sharp,[18] which includes the collective contributions, were used for the collective model calculations.

If the 2.08-Mev Na^{23} state is $3/2^+$ or $5/2^+$, the single-particle branching prediction is consistent with the observed value; if the state is $7/2^+$ the observed branching ratio is consistent with that predicted if substantial collective enhancement of the $E2$ radiation is present.

The small upper limit on the ground-state transition from the 2.70-Mev state precludes a $1/2^+$–$3/2^+$ combination for the 2.70- and 2.08-Mev states. Neglecting statistical factors, if the 2.70-Mev state is $3/2^+$ or $5/2^+$ and the 2.08-Mev state is either $3/2^+$ or $5/2^+$, then the $M1$ ground-state transition is inhibited by a factor of at least 550 relative to the 0.62-Mev $M1$ transition, based on the observed upper limit to the 2.70-Mev ground-state branch. This same inhibition holds if the 2.70-Mev state is $5/2^+$ and 2.08-Mev state is $7/2^+$. Therefore, the spin of the 2.70-Mev state must be $\geq7/2$.

[13] J. E. Mack, Revs. Modern Phys. **22**, 64 (1950); R. Berenbaum, J. H. Towle, and J. H. Matthews, Proc. Phys. Soc. (London) **A69**, 858 (1956); H. Hausman, J. E. Monahan, F. P. Mooring, and S. Raboy, Bull. Am. Phys. Soc. **1**, 56 (1956); R. W. Krone and W. G. Read, Bull. Am. Phys. Soc. **1**, 212 (1956); G. M. Temmer and N. P. Heydenburg, Phys. Rev. **104**, 967 (1956).

[14] J. R. Penning and F. H. Schmidt, Phys. Rev. **105**, 647 (1957).

[15] P. M. Endt and C. M. Braams, Revs. Modern Phys. **29**, 687 (1957).

[16] D. H. Wilkinson, *Proceedings of the Rehovoth Conference on Nuclear Structure*, edited by H. J. Lipkin (North-Holland Publishing Company, Amsterdam and Interscience Publishers, New York, 1958).

[17] S. G. Nilsson, Kgl. Danske Videnskab. Selskab., Mat.-fys. Medd. **29**, No. 16 (1955).

[18] D. A. Bromley, H. E. Gove, and A. E. Litherland, Can. J. Phys. **35**, 1057 (1957).

The upper limit on the ground-state branch from the 2.70-Mev state is consistent with a $7/2^+$ assignment to this state in combination with a $5/2^+$ assignment to the 2.08-Mev state; however, for this combination the 2.26-Mev $M1$ crossover transition suffers an inhibition of 150 relative to the $M1$ 0.62-Mev cascade transition. Such an inhibition is perhaps within the limits of straggling of "reduced $M1$ branching ratios" given by Wilkinson.[16] If the 2.70-Mev state is $9/2^+$ and the 2.08-Mev state is $7/2^+$, the $E2$ crossover transition is enhanced relative to the $M1$ cascade by a factor of about four, on the Weisskopf estimate. The observation of a transition to the $5/2^+$ 0.44-Mev state limits the spin of the 2.70-Mev state to $\leq 9/2$. It is concluded that the 2.70- and 2.08-Mev states are probably $9/2^+$ and $7/2^+$, respectively, although $7/2^+$ and $5/2^+$ are not completely precluded. A $7/2^+$ assignment for the 2.08-Mev state implies $5/2^+$ for the Ne^{23} ground state as expected both from the collective model and from the simple shell model.

Observation of ground-state branches from the Na^{23} states at 2.39-, 2.64-, 2.98-, and 3.92-Mev limit the spins of these states to $\leq 7/2$, with $7/2^-$ being excluded by the small rate for such an $M2$ transition compared with the competing $E1$ transition to the first excited state. Observation of cascade transitions to the $5/2^+$ first excited state similarly precludes $1/2^-$ for the 2.39-, 2.70-, 2.98-, and 3.68-Mev states. The absence of any strong transitions involving the 3.85-Mev state of Na^{23} suggests possible lack of population due to high spin. However, weak transitions to the ground or first excited state probably would be obscured by the 3.92- and 3.3-Mev gammas of Na^{23} and Ne^{20}, respectively. (The $3.85 \rightarrow 0.44$ Mev cascade gamma has been observed.[10]) Additional discussion of the spins of some of these states is given by Freeman and Montagu.[9]

The spin and parity of the Ne^{20} ground and first excited states are 0^+ and 2^+, respectively.[19] Observation of a gamma transition to the 4.97-Mev state from a 1^+ capturing state in the reaction $F^{19}+p \rightarrow Ne^{20}+\gamma$,[20] together with a triple angular correlation study, limits the spin and parity of the 4.97-Mev state to $1^\pm$, $2^\pm$, 3^+. The β-γ angular correlation in the allowed β decay of F^{20} to the 1.6-Mev state of Ne^{20} is consistent only with 2^+ for the F^{20} ground state.[21] The F^{20} β decay to the 4.97-Mev state of Ne^{20} is probably at least first forbidden, having $\log ft > 7$ from gamma-gamma coincidence measurements.[22] If this is so, the positive parity assignments are ruled out and the 4.97-Mev state of Ne^{20} would be 1^- or 2^-. An observable ground-state branch from this state would be consistent only with the 1^- assignment. The small upper limit set on such an $E1$ transition relative to a competing $E1$ cascade transition apparently favors the 2^- assignment. However, a 1^- assignment cannot be excluded, as the dominance of the cascade over the ground-state transition is within the limits given by Wilkinson.[16] An $M1$ ground-state transition from a 1^+ state at 13.5 Mev has been observed to be very strongly inhibited relative to the $M1$ cascade through the 1.6 Mev first excited state,[23] suggesting a substantial dissimilarity in the configurations of the ground and first excited states.

Recent studies of neutron angular distributions from the $F^{19}(d,n)$ reaction tentatively demonstrate stripping like patterns for certain states with $l=2$ or 3 for the 4.25 and $l=1$ for the 4.97-Mev states.[24] These results imply $I=1$, 2, 3, or 4 and positive parity for the 4.25-Mev state; $I=0$, 1 or 2 and negative parity for the 4.97-Mev state.

The reversal of sense of the anisotropy in the correlation of the Ne^{20} cascade gammas from the 4.2-Mev state renders a unique spin assignment impossible; however, the observed lack of isotropy rules out a zero spin for this state.

2. Collective Model Interpretation of the Na^{23} Levels

The observation of a large positive electric quadrupole moment for Na^{23} [25] implies a substantial shape deviation from spherical symmetry toward a prolate configuration, and suggests that collective effects may be expected in the level spectrum, moments, and beta and gamma transition probabilities. The large cross section for Coulomb excitation of the first excited state by protons and alpha particles[26] also implies substantial distortion. A theoretical study by Rakavy[1] suggests the systematic occurrence of large nuclear deformations between the closed shells of O^{16} and Si^{28}, and successful applications of the collective model have been made for this region of atomic number.[2] The applicability of the strong coupling collective model to the results obtained has therefore been considered.

It is expected from the prolate deformation eigenvalues of Nilsson's single-particle orbit solutions for a spheroidal potential well with spin-orbit coupling[17] that Na^{23} would have a ground state with a single unpaired proton having an angular momentum component $\Omega=3/2$ along the symmetry axis and positive parity, in agreement with the observed ground-state spin and parity, $3/2^+$. The prediction of the simple shell model, for short-range interparticle forces, is that the ground-state spin of an odd nucleus should be that of the

[19] G. Weinreich, G. Tucker, and V. Hughes, Phys. Rev. **87**, 229 (A) (1952).
[20] H. E. Gove, A. E. Litherland, and A. J. Ferguson, Bull. Am. Phys. Soc. **1**, 36 (1958).
[21] F. Boehm, V. Soergel, and B. Stech, Phys. Rev. Letters **1**, 77 (1958).
[22] R. W. Kavanagh, Bull. Am. Phys. Soc. **5**, 316 (1958), and private communication.
[23] A. B. Clegg, G. A. Jones and D. H. Wilkinson, Proc. Phys. Soc. (London) **A68**, 538 (1955).
[24] R. E. Benenson and L. J. Lidofsky, Bull. Am. Phys. Soc. **5**, 1 (1960).
[25] P. L. Sagalyn, Phys. Rev. **94**, 885 (1954); M. L. Perl, I. I. Rabi, and B. Senitzky, Phys. Rev. **98**, 611 (1955).
[26] G. M. Temmer and N. P. Heydenburg, Phys. Rev. **104**, 957 (1956).

unpaired nucleon[27] which, in Na^{23}, occupies a $d_{5/2}$ orbit. Abnormal coupling of the $(d_{5/2})^3$ proton configuration to a resultant spin of 3/2 might possibly be obtained for a reasonable force range; however, such an explanation fails to explain similar instances of abnormal coupling in $(f_{7/2})^3$ and $(g_{9/2})^3$ configurations.[28]

Low-lying positive parity states of single-particle excitation having $\Omega=1/2$ and 5/2 are also predicted. The simple collective model then predicts three bands of low-lying collective excited states of a rotational nature, each having one of the above intrinsic particle structures and characterized by a projection of the total angular momentum on the nuclear symmetry axis of $K=3/2$, 1/2, and 5/2, respectively. In the absence of perturbation, each band is expected to exhibit a characteristic level spacing given by

$$E_{K,I}=E_K{}^0+(\hbar^2/2F_K)[I(I+1)+\delta_{K,\frac{1}{2}}(-1)^{I+\frac{1}{2}}a(I+\tfrac{1}{2})],$$

where F_K is the effective moment of inertia and a the "decoupling parameter." [3]

For odd A nuclei this simple spectrum is expected to be substantially distorted by the coupling of the particle motion to the rotation of the potential well (rotation-particle coupling).[3,29] This "RPC" produces a mixing of the wave functions of the various bands among states having $\Delta I=0$, $\Delta K=\pm 1$. Another perturbation, which may be appreciable for high spin states, is due to the coupling of the low-lying states to highly excited collective states of a vibrational nature (rotation-vibration coupling).[3]

The RPC perturbation connects only states of the same parity for which $\Delta I=0$, $\Delta K=\pm 1$. For the case of Na^{23} there are thus three interacting bands expected, whose perturbed level positions for a given spin value are the roots of the cubic equation arising from the diagonalization of the appropriate 3×3 matrix, where the matrix elements for a specified nuclear deformation and spin-orbit coupling can be calculated from Nilsson's eigenfunctions.

The large number of adjustable parameters precludes a detailed fit to the model with available data. A plausible fit should be characterized by reasonable internal consistency of parameters and of the corresponding nuclear deformations, and by external consistency with the values of similar parameters for neighboring nuclei. A preliminary calculation of the level spectrum using the Nilsson eigenfunctions and making plausible assumptions has been made by Paul and Montagu,[30] who obtain a qualitative fit for levels up to 3 Mev using the same moment of inertia for all bands and a nuclear deformation derived from the measured ground-state quadrupole moment and the Coulomb excitation cross section for the $0\rightarrow 0.44$ Mev transition. These calculations predict that the first three states are $3/2^+$, $5/2^+$, and $7/2^+$ and that there is a low-lying $9/2^+$ state. The ground state and first excited state are known to be $3/2^+$ and $5/2^+$, respectively; the predicted $7/2^+$ and $9/2^+$ states may perhaps be identified with the states at 2.08 and 2.70 Mev, to which probable spins and parities of $7/2^+$ and $9/2^+$, respectively have been assigned. In addition, the calculations of Paul and Montagu predict $1/2^+$, $3/2^+$, and $5/2^+$ states below about 3.3 Mev, which are not inconsistent with our assignments of possible spins to the other states of this region.

The ground-state magnetic moment can be calculated as a function of distortion and spin-orbit coupling strength from the Nilsson eigenfunctions. Assuming the validity of the model, a comparison with the experimental value $\mu=2.216$ nm,[31] together with a knowledge of the distortion will, in principle, permit a determination of the spin-orbit coupling strength. The calculated magnetic moment for positive values of η is rather insensitive to the distortion, however, and since calculated magnetic moments are unreliable to 1/4–1/2 nuclear magneton due to uncertain mesonic contributions,[32] this procedure does not yield any useful information on spin-orbit coupling. Similarly, the calculated ft value for the Mg^{23} mirror beta decay does not yield any spin-orbit information due to experimental uncertainties and the insensitivity of the calculated value to positive deformations. Uncertainty in g_R increases the uncertainty in these quantities.

For pure rotational states, the $M1$ and $E2$ gamma-ray transition probabilities can be expressed in terms of the quadrupole moment and magnetic moment of the lowest member, with an assumption as to the value of g_R, the gyromagnetic ratio of the rotational motion. The decay rates shown in Table IV were calculated for the indicated spin assumptions for a pure $K=3/2$ rotational band, assuming $g_R\approx 0.2$.

The gamma ray from the 0.44-Mev state to the ground state is predicted to be largely $M1$ by both single-particle and collective models. A limit of 0.05 has been put on the $E2$ to $M1$ ratio for this transition by Berenbaum *et al.*[13] The ground-state transition for the 2.08-Mev state (assumed $7/2^+$) is stronger than predicted by the Weisskopf model and may exhibit the $E2$ enhancement characteristic of collective transitions. Agreement with the Nilsson collective model predictions is good. For the 2.70-Mev state (assumed $9/2^+$), however, the collective model predicts that the $E2$ crossover transition should be much stronger (approximately 10 times) than the $M1$ cascade, whereas agreement is fair between the observed branches and

[27] M. G. Mayer, Phys. Rev. **78**, 22 (1950).
[28] D. Kurath, Phys. Rev. **80**, 98 (1950); A. R. Edmonds and B. H. Flowers, Proc. Roy. Soc. (London) **214**, 515 (1952); I. Talmi, Helv. Phys. Acta **25**, 185 (1952).
[29] A. K. Kerman, Kgl. Danske Videnskab. Selskab., Mat.-fys. Medd. **30**, No. 15 (1956).
[30] E. B. Paul and J. H. Montagu, Nuclear Phys. **8**, 61 (1958).
[31] *A Table of Nuclear Moment Data*, edited by H. E. Walchli, Oak Ridge National Laboratory Report ORNL-1469, 1953 (unpublished).
[32] R. J. Blin-Stoyle, Revs. Modern Phys. **28**, 75 (1956).

the single-particle predictions. This discrepancy with the predictions of the collective model might be due to reduction of matrix elements owing to the rotational band admixtures expected for these states.

3. Significance of the Ne^{20} Results

The characteristics of the first few excited states of Ne^{20} are of interest for possible nuclear model interpretation and for astrophysical calculations. The state at 4.97 Mev may correspond to a resonance in the capture reaction $O^{16}+\alpha \rightarrow Ne^{20*} \rightarrow Ne^{20}+\gamma$, provided that its parity is $(-1)^I$. Following hydrogen exhaustion, such a reaction is postulated in a helium burning process within the helium rich core of red giant stars.[33] A spin-parity assignment of 1^- or 2^+ to this state would imply that the capture reaction can occur and conversely for a 2^- or 3^+ assignment. According to calculations of Cameron,[4] for a 1^- assignment large amounts of Ne^{20} can be formed in the latter stages of helium burning even for values of the alpha-particle reduced width as small as 0.01 of the Wigner limit. It has also been suggested that Ne^{20} may play an important role in the production of neutrons for synthesis of intermediate and heavy elements, via the reactions $Ne^{20}+p \rightarrow Na^{21}+\gamma$; $Na^{21} \rightarrow Ne^{21}+\beta^+ +\nu$; $Ne^{21}+\alpha \rightarrow Mg^{24}+n$.[5] Production of heavier alpha-particle nuclei via the reactions $Ne^{20}+\gamma \rightarrow O^{16}+\alpha$; $Ne^{20}+\alpha \rightarrow Mg^{24}+\gamma$ has been suggested to occur at temperatures of about 10^9 °K.[5]

For the 0^+ Ne^{20} ground state, no static quadrupole moment is expected. However, the short lifetime $[(5.3\pm2.3)\times10^{-13}$ sec] of the 2^+ 1.63-Mev state[34] suggests an enhanced $E2$ transition rate and a correspondingly large nuclear deformation, as predicted by Rakavy.[1] An intrinsic quadrupole moment $Q_0 \sim 0.67$ barn is implied by this lifetime.

Paul has given a rotational interpretation of the level spectrum of F^{19} on the collective model,[35] obtaining results similar to those obtained from shell-model calculations in terms of configuration mixing for intermediate coupling. A prolate configuration is required in this calculation in order to obtain agreement with the observed spectrum. Furthermore, a positive quadrupole moment has recently been measured for Ne^{21}.[36] Thus Ne^{20} might also be expected to have a prolate deformation, as predicted by Rakavy.

VI. SUMMARY AND CONCLUSIONS

Gamma-ray decay schemes and branching ratios have been obtained for excited states of Na^{23} and Ne^{20} using scintillation spectrometry, including a three-crystal pair detector, gamma-gamma and particle-gamma coincidence arrangements, and large single-crystal detectors.

Probable spin and parity assignments for the Na^{23} levels at 2.08 Mev and 2.70 Mev are $7/2^+$ and $9/2^+$, respectively, although a $5/2^+ - 7/2^+$ combination cannot be completely excluded. Spin limitations on other states of Na^{23} are: 2.39-, 2.64-, 2.98-, and 3.92-Mev states, $\leq 7/2$ with $7/2^-$ excluded and $1/2^-$ excluded for the 2.39- and 2.98-Mev states; $1/2^-$ is excluded for the 2.70- and 3.68-Mev state. These spin-parity assignments, along with other data, are consistent with a collective interpretation in terms of the strong-coupling rotational model, with large perturbations among the low-lying bands.

The upper limit of 4% for the ground-state branch of the 4.97-Mev state of Ne^{20}, together with other data, is suggestive of a 1^- or 2^- assignment, with 2^- the more likely. Other assignments are not definitely excluded. A 9% upper limit is placed on the ground-state branch of the Ne^{20} 4.2-Mev state. Spin zero is excluded for this state.

ACKNOWLEDGMENTS

One of us (T. H. K.) wishes to express his appreciation of partial financial support furnished by the Carbide and Carbon Chemicals Company through the Carbide and Carbon Chemicals Company Fellowship in Physics for the academic year 1956–1957.

[33] E. E. Salpeter, Phys. Rev. **107**, 516 (1957).
[34] S. Devons, G. Manning, and J. H. Towle, Proc. Phys. Soc. (London) **A69**, 173 (1956).
[35] E. B. Paul, Physica **22**, 1140 (1956).
[36] G. M. Grosof, P. Buck, W. Lichten, and I. I. Rabi, Phys. Rev. Letters **1**, 214 (1958).